D-^{18}F-Fluoromethyl Tyrosine Imaging of Bone Metastases in a Mouse Model

Sabine Zitzmann-Kolbe[1], Anne Strube[1], Anna-Lena Frisk[1], Sanna-Maria Käkönen[1,2], Hideo Tsukada[3], Peter Hauff[1], Dietmar Berndorff[1], and Keith Graham[1]

[1]Global Drug Discovery, Bayer Schering Pharma AG, Berlin, Germany; [2]Department of Cell Biology and Anatomy, University of Turku, Turku, Finland; and [3]Central Research Laboratory, Hamamatsu Photonics, Hamamatsu, Japan

The presence and localization of metastatic bone lesions is important for the staging of the disease and subsequent treatment decisions. Detecting tumor cells would have additional value over the current indirect bone scintigraphy method for detecting areas of elevated skeletal metabolic activity. D-^{18}F-fluoromethyl tyrosine (D-^{18}F-FMT) has recently shown good uptake and fast elimination, resulting in good tumor-to-background ratios. The potential of D-^{18}F-FMT for imaging bone metastases has been investigated. **Methods:** 786-O/luciferase human renal adenocarcinoma cells were injected intracardially, resulting in the formation of bone metastases in mice. Small-animal PET was performed 51 and 65 d after tumor cell inoculation. **Results:** D-^{18}F-FMT showed specific uptake in the bone metastases, giving excellent images with a little background in the pancreas. All imaged metastases were histologically confirmed. A bone scan with ^{18}F-fluoride showed elevated skeletal metabolic activity in the areas of osteolytic lesions. **Conclusion:** D-^{18}F-FMT is a useful PET tracer for the detection of bone metastases and should be evaluated in the clinical setting.

Key Words: PET/CT; D-^{18}F-FMT; ^{18}F-fluoride; imaging; bone metastases; tyrosine

J Nucl Med 2010; 51:1632–1636
DOI: 10.2967/jnumed.110.078899

The presence and localization of metastatic bone lesions is important for the staging of the disease and subsequent treatment decisions. Detecting tumor cells would have additional value over the current indirect bone scintigraphy method for detecting areas of elevated skeletal metabolic activity (*1*). ^{18}F-FDG and ^{18}F-fluoride are under investigation as PET tracers for the detection of bone metastases. Amino acids are important biologic substrates, which play crucial roles in virtually all biologic processes. Amino acids accumulate in malignant transformed cells because of increased expression of amino acid transporters (*2*). One important amino acid transporter is the L-type amino acid transporter 1, which transports large neutral amino acids (*3*). Preliminary studies using ^{11}C-methionine gave mixed results in patients with bone metastases. One study reported good detection of breast cancer bone metastases with ^{11}C-methionine and even detected 5 new lesions (*4*), whereas another study using a heterogeneous mixed-tumor patient population showed an overall bone metastasis detection rate of 56.5% for PET and 23.1% for bone scintigraphy (*5*).

L-type amino acid transporter 1 is highly expressed in many tumors and tumor cell lines of various origins (*6,7*). In a study with 321 patients investigating lung tumors, 29% of adenocarcinoma cases, 91% of squamous cell carcinoma cases, and 67% of large cell carcinoma cases were positive for L-type amino acid transporter 1 protein expression. This expression positively correlated with the proliferation marker Ki-67 (*8*). Various ^{18}F-labeled tyrosine derivatives have been synthesized to explore the L-transporter system for PET tumor imaging: *O*-(2-^{18}F-fluoroethyl)-L-tyrosine (^{18}F-L-FET) is gaining more attention for the clinical imaging of primarily gliomas (*9*), and L-3-^{18}F-fluoro-α-methyltyrosine showed positive uptake in 84% of all cancers (31/37 patients) in a study of thoracic tumors (*10*). The idea of using D-isomers of amino acids for imaging was successfully introduced by Tsukada et al. for PET tracers (*11,12*) and Kersemans et al. for SPECT tracers (*13*); these studies showed that D-tyrosine derivatives have advantages over their L-counterparts. In particular, D-^{18}F-fluoromethyl tyrosine (D-^{18}F-FMT) showed good uptake into HeLa tumors and exhibited faster elimination rates than the corresponding L-isomer, leading to improved tumor-to-nontumor ratios. Studies on the uptake and excretion of L- and D-^{18}F-FMT suggest a difference in the influence of extracellular amino acids between ^{18}F-L- and D-^{18}F-FMT (*14*). In addition, D-^{18}F-FMT was successful in monitoring the response of tumors to radiotherapy in the murine squamous cell carcinoma cell line SCCVII tumor–bearing mice (*15*).

In this study, we investigated the potential of D-^{18}F-FMT to image bone metastases in a mouse model. Injection of 786-O/luciferase cells into the arterial circulation resulted in the development of aggressive osteolytic lesions in bones within 62 ± 8 d. The tumors were primarily located within the bone and resulted in cortical destruction of the bone. No soft-tissue metastases (kidneys, adrenal glands, heart,

Received May 10, 2010; revision accepted Jul. 20, 2010.
For correspondence or reprints contact: Sabine Zitzmann-Kolbe, Bayer Schering Pharma AG, Research Laboratories, Müllerstrasse 178, D-13342 Berlin, Germany.
E-mail: sabine.zitzmann-kolbe@bayerhealthcare.com

lungs) were detected by bioluminescence imaging or by histomorphometry (*16*). A bone scan with ^{18}F-fluoride was obtained and histologic determination was performed to validate the localization of the bone metastases.

MATERIALS AND METHODS

Cell Line

The 786-O/luciferase cell line was generated by stable transfection with a pRev CMV_luc2 vector. The cells were cultured in RPMI medium (Biochrom AG) containing 10% heat-inactivated fetal calf serum (Biochrom AG), 2% glutamine (PPA Laboratories), 4.5 g of glucose per liter (Sigma-Aldrich Chemie GmbH), 10 mM *N*-(2-hydroxyethyl)piperazine-*N*′-(2-ethanesulfonic acid) (Biochrom AG), 1 mM pyruvate (Biochrom AG), and 50 μg hygromycin B per milliliter (Invitrogen Ltd.).

Animals and Tumor Growth

786-O/luciferase cells were harvested from subconfluent cell culture flasks and resuspended in phosphate-buffered saline (Biochrom AG) to a final concentration of 5×10^5 cells/100 μL. We used an insulin syringe (BD Micro-Fine+Demi U-100; Becton Dickinson GmbH) to inoculate 5×10^5 786-O/luciferase cells in 100 μL of phosphate-buffered saline into the left cardiac ventricle of anesthetized 5-wk-old female athymic nude mice (Harlan-Winkelmann GmbH) (*16*). Experiments were approved by the governmental review committee on animal care.

Optical Imaging

Tumor cell dissemination in bone was regularly monitored by bioluminescence imaging using a cooled charge-coupled device camera (NightOWL LB; Berthold Technologies). The mice were injected intravenously with 100 μL of luciferin (45 mg/mL in phosphate-buffered saline; Synchem OHG) and anesthetized with 1%–3% isoflurane (CuraMED Pharma GmbH). Photon emission was measured over an integration of 20 s and recorded as pseudocolor images that were quantified using WinLight software (Berthold Technologies).

Radiosynthesis of D-^{18}F-FMT

D-^{18}F-FMT was synthesized as previously described (*12*). In brief, ^{18}F-fluoride (34.2 GBq) was eluted from a QMA (Waters) cartridge. The ^{18}F-fluoride was eluted with a solution of K_2CO_3 (2.7 mg) in 50 μL of water and K222 (15 mg) in 950 μL of acetonitrile. This solution was dried at 120°C under a vacuum and a stream of nitrogen. Additional acetonitrile (1 mL) was added and the drying step was repeated. Dibromomethane (100 μL) in acetonitrile (900 μL) was added and heated at 130°C for 5 min. The reaction was cooled and ^{18}F-fluoromethylbromide was distilled under a nitrogen flow of 50 mL/min through 4 Silica Plus (Waters) cartridges connected in series into a solution of D-tyrosine (3 mg) in dimethyl sulfoxide (1 mL) with 10% NaOH (13.5 μL). This solution was heated at 110°C for 5 min and then cooled to 40°C. The D-^{18}F-FMT was purified by semipreparative high-performance liquid chromatography (Synergi Hydro RP 4 μm, 250 × 10 mm [Phenomenex]; 10% acetonitrile in water at pH 2; flow, 5 mL/min). The product peak was collected, diluted with water (20 mL, pH 2), and passed through a C18 Plus Environmental (Waters) cartridge, which was then washed with water of pH 2 (5 mL). D-^{18}F-FMT was eluted with EtOH:water (1:1; pH 2, 3 mL) to give 3.2 GBq (15% d.c.) of D-^{18}F-FMT with a specific activity of 49 GBq/μmol in a synthesis time of 71 min.

PET/CT and Data Reconstruction

Ten to 12 MBq of ^{18}F-fluoride (Eckert and Ziegler) or D-^{18}F-FMT were injected into the tail vein. Sixty minutes after injection, anesthesia was induced by isoflurane and O_2, followed by 20-min micro-PET/CT scans using an Inveon embedded PET/CT scanner (Siemens). Settings for CT were a 360° scan, 180 projections, hardware binning of 2, 1,100-ms exposure time, and x-ray source of 80 kV and 500 μA. Settings for PET were an acquisition time of 1,200 s with a static histogram. We used an Inveon Research Workplace with multimodality 3-dimensional visualization for CT surface rendering and PET volume rendering. Reconstruction was done with 2-dimensional ordered-subset expectation maximization, with a 128 × 128 matrix and 4 iterations.

Histologic Examination

After the PET/CT measurement, the mice were sacrificed by an overdose of isoflurane and O_2. With the information from the PET images, the bones that showed D-^{18}F-FMT were removed. After fixation in 4% neutral-buffered formalin and decalcification, the samples were embedded in paraffin and sections were stained with hematoxylin and eosin for microscopic examination. Immunohistochemistry for the detection of pancytokeratin (AE1/AE3, ab27988; Abcam), which recognizes epitopes present in epithelial tissues, was performed to identify the origin of the tumor cells (epithelial vs. nonepithelial). For differential localization of osteoid and collagen, slides were stained with Masson–Goldner trichrome (Merck).

RESULTS

The detection of bone metastases with D-^{18}F-FMT was preclinically investigated in the 786-O/luciferase human renal cell adenocarcinoma bone metastasis mouse model.

In vitro experiments showed good uptake of D-^{18}F-FMT into the 786-O/luciferase cells, reaching 12.8% applied dose/10^6 cells after 30 min (data not shown).

The luciferase gene–transfected 786-O cells offer a reliable tool for following bone metastasis formation in vivo by longitudinal whole-body bioluminescence imaging. Bioluminescence was used to monitor metastasis progression, and tumor growth was observed in the regions of hind limbs, forelimbs, spine, and skull (Fig. 1). All hot spots seen in these images represent accumulation of tumor cells expressing the luciferase gene.

Fifty-one days after the inoculation of the 786-O/luciferase cells, PET/CT was performed with ^{18}F-fluoride (Fig. 2, right). The images showed high accumulation in multiple osteolytic lesions in the spine, skull, forelimbs, and hind limbs, indicating increased skeletal metabolic activity, compared with the uptake in healthy bone. The same mouse was imaged 2 wk later (day 65) with D-^{18}F-FMT (Fig. 2, left), and the same bone lesions previously visualized with ^{18}F-fluoride and additional lesions were visible. Thus, the localization of tumor cells monitored by D-^{18}F-FMT correlated with the affected areas of the skeleton visualized with ^{18}F-fluoride. D-^{18}F-FMT also showed pancreas uptake, which is consistent with the literature. The calculation of percentage injected dose per gram based on the standardized uptake value was between 4.1 and 6.8 for

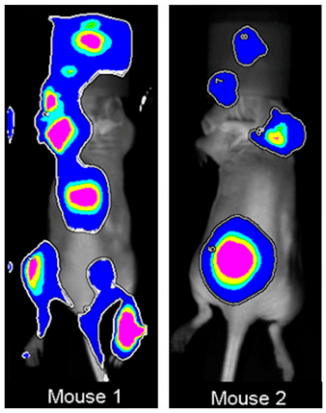

FIGURE 1. Representative bioluminescence images (dorsal view) of 2 mice inoculated intracardially with human 786-O/luciferase cells. 65 d (mouse 1) and 55 d (mouse 2) after inoculation, spread of cancer cells is evident in hind limbs, forelimbs, spine, and skull.

the various lesions, and the average was 5.7 ± 0.68 percentage injected dose per gram. The size of the metastases ranged from 4.2 to 82.6 mm^3 in volume, as determined from PET signals. D-^{18}F-FMT showed no uptake into the healthy bone.

Reconstruction of the CT and PET images by surface rendering showed extensive bone destruction caused by tumor cells (Fig. 3, left). The PET signal (Fig. 3, middle) showed a specific localization in the areas of osteolytic lesions after the fusion of PET and CT images (Fig. 3, right). Additionally, PET was able to visualize small lesions (e.g., in the shoulder blade), whereas the CT images were inconclusive.

Histologically, the hematopoietic cell areas were entirely replaced by tumor tissue in the medullary cavity in all samples collected after the PET/CT. The proliferating cells were large and pleomorphic, with abounded cytoplasm and round dense nuclei; in other areas spindle-shaped cells separated by a moderate amount of collagenous matrix were more predominant (Fig. 4). A moderate number of mitotic figures were present (0–3 at ×40). Multinucleated giant cells were present within the tumor masses. These cells are probably osteoclasts (as shown with staining with tartrate-resistant acid phosphatase (*17*)); however, it cannot be excluded that these cells are pleomorphic polynucleated tumor cells because they are not adjacent to the bone and they differ morphologically from normal osteoclasts. An essential feature of the tumors was the lysis of normal bone, which occurred simultaneously with the formation of new osteoids. These osteoids stained blue green with Masson–Goldner trichrome (Supplemental Fig. 1; supplemental materials are available online only at http://jnm.snmjournals.org). Because the tumor had some morphologic similarities to a bone tumor, pancytokeratin staining was performed to confirm the epithelial origin of the metastases.

DISCUSSION

In our experiments, we could clearly show the ability of D-^{18}F-FMT to detect bone metastases in a nude mouse model.

The areas of the bone that showed D-^{18}F-FMT accumulation were removed and histologically examined. Tumor cells were detected, which had invaded the bones and were most likely responsible for the D-^{18}F-FMT accumulation. Because ^{18}F-FDG shows considerable uptake into inflammatory lesions, a particular focus within the histologic examinations was to differentiate between tumor and inflammatory lesions. Histologic examination of the areas in which D-^{18}F-FMT accumulated showed no signs of inflammation or invasion of macrophages. It is unlikely that the accumulation of D-^{18}F-FMT is caused by the uptake into immune cells. Tsukada et al. (*12*) demonstrated in a turpentine-induced inflammation model that D-^{18}F-FMT showed no uptake in inflammatory muscle tissue, in contrast to ^{18}F-FDG. In other mouse tumor models, we could histologically confirm different inflammatory sites that were positive for ^{18}F-FDG uptake but negative for D-^{18}F-FMT uptake (data not shown).

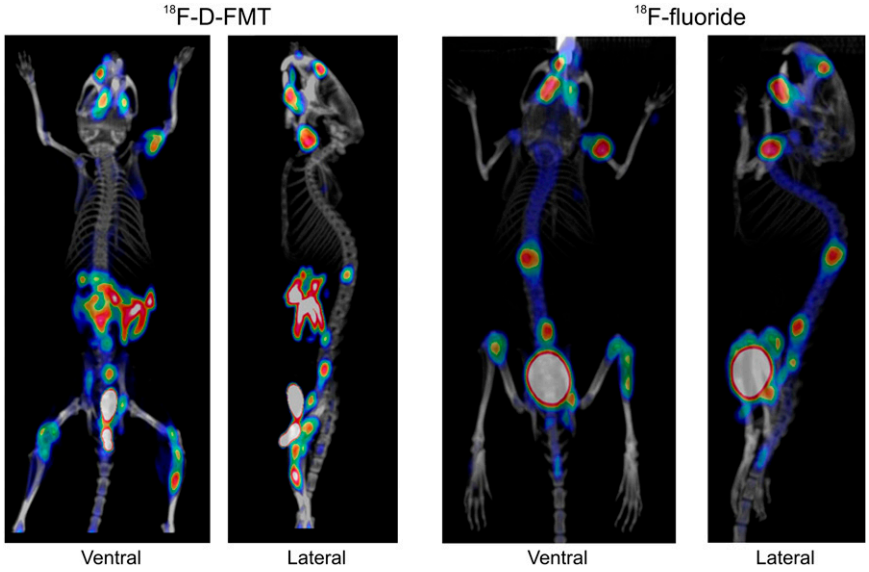

FIGURE 2. PET/CT images of D-^{18}F-FMT and ^{18}F-fluoride from mouse with 786-O/luciferase bone metastases. Scans were obtained 2 wk apart—first ^{18}F-fluoride scan and then D-^{18}F-FMT scan. D-^{18}F-FMT accumulates in tumor cells, and ^{18}F-fluoride is incorporated into regenerating bone.

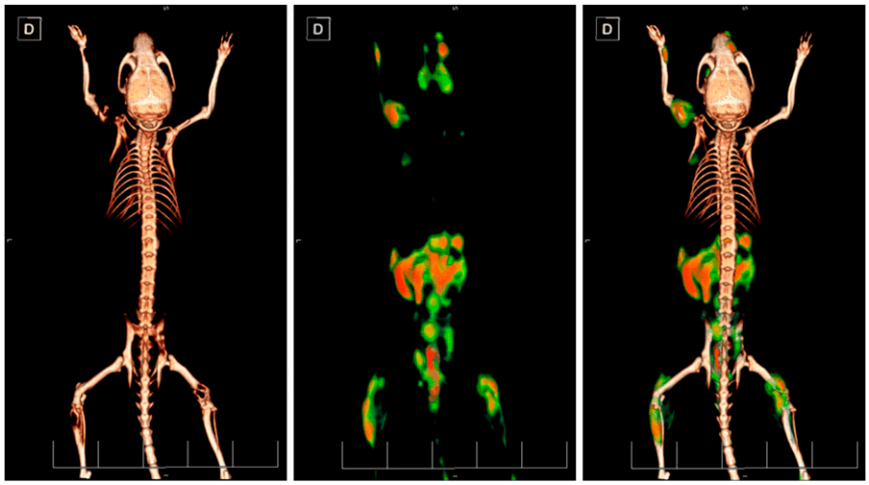

FIGURE 3. PET/CT images of D-^{18}F-FMT from mouse with 786-O/luciferase bone metastases (left image, CT; middle image, PET; right image, PET/CT fusion). CT images were calculated using surface-rendering program. Images show dorsal view.

In our PET scans, D-^{18}F-FMT showed abdominal retention due to uptake into the pancreas, which is similar to previous findings (*11*). This high pancreas uptake in mice has also been reported for ^{18}F-L-FET (*18*). However, human studies have shown low pancreas uptake of L-FET; the reason for this species difference remains unclear (*9*).

Interestingly, we could also detect the osteolytic bone metastases with ^{18}F-fluoride, indicating an increased metabolic activity in the affected bones areas. As shown histologically, bone destruction occurs in addition to new bone formation; whether this new bone formation is induced directly by tumor cells or indirectly by growth factors need to be further investigated. ^{18}F-fluoride is known to be incorporated into apatite molecules in exchange for a hydroxy group; this ^{18}F-fluoride uptake has been observed in regenerating and remineralizing bone and is therefore unspecific (*19*). In our studies, the larger bones (spine, legs) and joints also showed increased ^{18}F-fluoride uptake. Our results

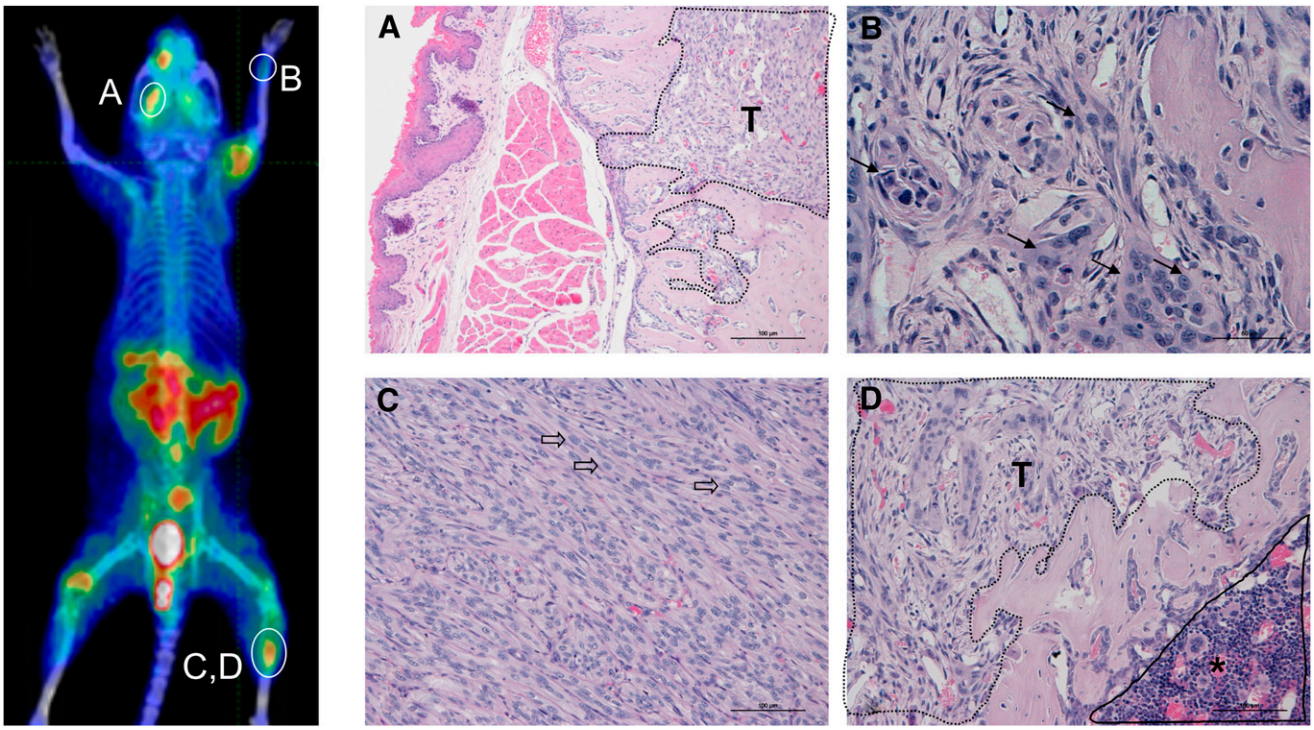

FIGURE 4. PET/CT images of D-^{18}F-FMT and ^{18}F-fluoride from mouse with 786-O/luciferase bone metastases, and corresponding histopathologic lesions. Hematopoietic cell areas are entirely replaced by tumor tissue (encircled T) in medullary cavity (A and D). (B) Area with large tumor cells (arrows) is seen. (C) Tumor is composed of spindle cells (block arrows). (D) Area of hematopoietic cells is still present (encircled *) beside tumor mass (T).

agree with those of Berger et al. (*20*), in which osseous lesions were detected with ^{18}F-fluoride, but not with those of Franzius et al. (*21*), in which bone metastases derived from human Ewing tumors showed a reduced uptake of ^{18}F-fluoride. These findings indicate that only certain types of osseous lesions show ^{18}F-fluoride accumulation, and further investigations on this subject are warranted.

A comparison of the PET/CT scans of ^{18}F-fluoride and D-^{18}F-FMT clearly shows accumulation of D-^{18}F-FMT in all of the bone metastases, plus several more lesions (lower spine, front leg), imaged by ^{18}F-fluoride. These additional metastases might have grown in the 2 wk between the 2 scans or could represent early metastases, which show tumor cell invasion but not current bone regeneration. This new tracer, D-^{18}F-FMT, offers an opportunity to further address this interesting question.

CONCLUSION

In addition to the already published use of D-^{18}F-FMT to detect solid tumors, this tracer also offers the possibility to detect bone metastases and possibly soft-tissue metastases.

ACKNOWLEDGMENTS

We acknowledge the contributions of Selahattin Ede and Mario Mandau for the radiolabeling of D-^{18}F-FMT, Eva-Maria Bickel for PET/CT, Bernd Hartmann for the intracardiac inoculations, and Andreas Kolbe for information technology support.

REFERENCES

1. Chua S, Gnanasegaran G, Cook GJ. Miscellaneous cancers (lung, thyroid, renal cancer, myeloma, and neuroendocrine tumors): role of SPECT and PET in imaging bone metastases. *Semin Nucl Med.* 2009;39:416–430.
2. Christensen HN. Role of amino acid transport and countertransport in nutrition and metabolism. *Physiol Rev.* 1990;70:43–77.
3. Yanagida O, Kanai Y, Chairoungdua A, et al. Human L-type amino acid transporter 1 (LAT1): characterization of function and expression in tumor cell lines. *Biochim Biophys Acta.* 2001;1514:291–302.
4. Lindholm P, Lapela M, Nagren K, Lehikoinen P, Minn H, Jyrkkio S. Preliminary study of carbon-11 methionine PET in the evaluation of early response to therapy in advanced breast cancer. *Nucl Med Commun.* 2009;30:30–36.
5. Goudarzi B, Kishimoto R, Komatsu S, et al. Detection of bone metastases using diffusion weighted magnetic resonance imaging: comparison with ^{11}C-methionine PET and bone scintigraphy. *Magn Reson Imaging.* 2010;28:372–379.
6. Kobayashi H, Ishii Y, Takayama T. Expression of L-type amino acid transporter 1 (LAT1) in esophageal carcinoma. *J Surg Oncol.* 2005;90:233–238.
7. Nawashiro H, Otani N, Shinomiya N, et al. L-type amino acid transporter 1 as a potential molecular target in human astrocytic tumors. *Int J Cancer.* 2006;119:484–492.
8. Kaira K, Oriuchi N, Imai H, et al. Prognostic significance of L-type amino acid transporter 1 expression in resectable stage I-III nonsmall cell lung cancer. *Br J Cancer.* 2008;98:742–748.
9. Langen KJ, Hamacher K, Weckesser M, et al. *O*-(2-[^{18}F]fluoroethyl)-L-tyrosine: uptake mechanisms and clinical applications. *Nucl Med Biol.* 2006;33:287–294.
10. Kaira K, Oriuchi N, Shimizu K, et al. Evaluation of thoracic tumors with ^{18}F-FMT and ^{18}F-FDG PET-CT: a clinicopathological study. *Int J Cancer.* 2009; 124:1152–1160.
11. Tsukada H, Sato K, Fukumoto D, Kakiuchi T. Evaluation of D-isomers of *O*-^{18}F-fluoromethyl, *O*-^{18}F-fluoroethyl and *O*-^{18}F-fluoropropyl tyrosine as tumour imaging agents in mice. *Eur J Nucl Med Mol Imaging.* 2006;33:1017–1024.
12. Tsukada H, Sato K, Fukumoto D, Nishiyama S, Harada N, Kakiuchi T. Evaluation of D-isomers of *O*-^{11}C-methyl tyrosine and *O*-^{18}F-fluoromethyl tyrosine as tumor-imaging agents in tumor-bearing mice: comparison with L- and D-^{11}C-methionine. *J Nucl Med.* 2006;47:679–688.
13. Kersemans V, Cornelissen B, Bacher K, et al. In vivo evaluation and dosimetry of ^{123}I-2-iodo-D-phenylalanine, a new potential tumor-specific tracer for SPECT, in an R1M rhabdomyosarcoma athymic mouse model. *J Nucl Med.* 2005;46:2104–2111.
14. Urakami T, Sakai K, Asai T, Fukumoto D, Tsukada H, Oku N. Evaluation of *O*-[^{18}F]fluoromethyl-d-tyrosine as a radiotracer for tumor imaging with positron emission tomography. *Nucl Med Biol.* 2009;36:295–303.
15. Murayama C, Harada N, Kakiuchi T, et al. Evaluation of D-^{18}F-FMT, ^{18}F-FDG, L-^{11}C-MET, and ^{18}F-FLT for monitoring the response of tumors to radiotherapy in mice. *J Nucl Med.* 2009;50:290–295.
16. Strube A, Stepina E, Hartmann B, Neumann I, Hauff P, Kaekoenen S. P14. Development and characterization of a new renal cell carcinoma (RCC) bone metastasis mouse model. *Cancer Treat Rev.* 2008;34(suppl 1):17.
17. Strube A, Stepina E, Mumberg D, Scholz A, Hauff P, Kakonen SM. Characterization of a new renal cell carcinoma bone metastasis mouse model. *Clin Exp Metastasis.* 2010;27:319–330.
18. Wester HJ, Herz M, Weber W, et al. Synthesis and radiopharmacology of *O*-(2-[^{18}F]fluoroethyl)-L-tyrosine for tumor imaging. *J Nucl Med.* 1999;40:205–212.
19. Schirrmeister H. Detection of bone metastases in breast cancer by positron emission tomography. *Radiol Clin North Am.* 2007;45:669–676.
20. Berger F, Lee YP, Loening AM, et al. Whole-body skeletal imaging in mice utilizing microPET: optimization of reproducibility and applications in animal models of bone disease. *Eur J Nucl Med Mol Imaging.* 2002;29:1225–1236.
21. Franzius C, Hotfilder M, Poremba C, et al. Successful high-resolution animal positron emission tomography of human Ewing tumours and their metastases in a murine xenograft model. *Eur J Nucl Med Mol Imaging.* 2006;33:1432–1441.